# Defining Radiation Belt Enhancement Events Based on Probability Distributions

Geoffrey D. Reeves[1,2], Elizabeth M. Vandegriff[2], Jonathan T. Niehof[3], Steven K. Morley[1], Gregory S. Cunningham[1], Michael G. Henderson[1], and Brian A. Larsen[1,2]

1) Space Science and Applications Group, Los Alamos National Laboratory, Los Alamos, NM 87545

2) The New Mexico Consortium, Los Alamos, NM 87544

3) The University of New Hampshire, Durham, NH 03824

correspondence to Geoff Reeves, Geoff@reevesresearch.org 505-500-5106

## Abstract

We present a methodology to define strong, moderate, and intense space weather events based on probability distributions. We have illustrated this methodology using a long-duration, uniform data set of 1.8-3.5 MeV electron fluxes from multiple LANL geosynchronous satellite instruments but a strength of this methodology is that it can be applied uniformly to heterogeneous data sets. It allows quantitative comparison of data sets with different energies, units, orbits, etc. The methodology identifies a range of times, "events", using variable flux thresholds to determine average event occurrence in arbitrary 11-year intervals ("cycles"). We define strong, moderate, and intense events as those that occur 100, 10, and 1 time per cycle and identify the flux thresholds that produce those occurrence frequencies. The methodology does not depend on any ancillary data set (e.g. solar wind or geomagnetic conditions). We show event probabilities using GOES > 2 MeV fluxes and compare them against event probabilities using LANL 1.8-3.5 MeV fluxes. We present some examples of how the methodology picks out strong, moderate, and intense events and how those events are distributed in time: 1989 through 2018, which includes the declining phases of solar cycles 22, 23, and 24. We also provide

an illustrative comparison of moderate and strong events identified in the geosynchronous data with Van Allen Probes observations across all L-shells. We also provide a catalog of start and stop times of strong, moderate, and intense events that can be used for future studies.

## 1. Introduction

Radiation belt electron fluxes undergo periods of rapid enhancement followed by more gradual decay. Therefore, periods of high fluxes are often described as "events" that typically last for several days to weeks (depending in part on the definition of an "event"). There are several reasons why it is valuable to have a quantitative definition of radiation belt electron events including historical studies of spacecraft operational anomalies, statistical studies of the processes that enhance or deplete radiation belt fluxes, real-time identification of enhancement events, quantitative definition of event criteria for forecasting, and others.

There are, however, a number of factors that make it difficult to develop a standard definition of radiation belt enhancement events. NOAA issues an Electron Event Alert when the >2 MeV electron flux measured by the geosynchronous GOES satellites exceeds $10^3$ particles/(cm$^2$-s-sr). NOAA's objective, however, is to provide advance or current warning of hazardous conditions rather than providing a historical catalog of events. Furthermore, NOAA's event threshold is highly specific to the GOES measurements. It only applies to geosynchronous >2 MeV integral fluxes, i.e. particles/(cm$^2$-s-sr). It is not generally possible to apply the same criteria to other measurements, even at geosynchronous orbit. The LANL geosynchronous measurements, for example, have different energy thresholds and are differential measurements; e.g. 1.8-3.5 MeV in units of particles/(cm$^2$-s-sr-keV) [*Reeves et al.*, 1996]. Similarly, the Van Allen Probes MagEIS and REPT instruments also provide differential flux measurements but with still different energy thresholds [*Baker et al.*, 2012; *Blake et al.*, 2013; *Spence et al.*, 2013]. It would also be valuable to be able to identify events using other long-term data sets such as GPS [*Morley et al.*, 2016], Polar [*Blake et al.*, 1995], SAMPEX [*Baker et al.*, 1993] and others.

A number of statistical studies have used geomagnetic or solar wind parameters to study radiation belt electron enhancement events. For example, [*Reeves et al.*, 2003] examined all times when the Dst index dropped below -50 nT to study whether storms enhanced or depleted the radiation belts. [See also *Anderson et al.*, 2015; *Kilpua et al.*, 2015; *Moya et al.*, 2017; *Turner et al.*, 2019.] Another set of papers starts with specific solar wind conditions such as CMEs or High-Speed Streams and investigates the radiation belt response [e.g. *Borovsky and Denton*, 2006; *Miyoshi and Kataoka*, 2008; *Shen et al.*, 2017; *Benacquista et al.*, 2018; *Bingham et al.*, 2019]. In addition to these types of studies, it would be valuable to be able to start with a set of defined radiation belt enhancement events and ask "What are the associated geomagnetic and/or solar wind conditions?". In particular an enhancement event list could be used to identify the range of conditions that produce enhancements and determine how uniquely those conditions (or processes) lead to radiation belt enhancement events.

In this paper we describe a methodology based on probability distributions that can be used to identify radiation belt enhancement events using only electron flux data. We illustrate the methodology using geosynchronous, ~2 MeV, daily-averaged electron fluxes but show how the same methodology could be applied to a wide variety of heterogenous data sets using different energies, different instrument response parameters, or different satellite orbits. We also present a catalog of events that can be used for further scientific studies (section 6).

## 2. Methodology

In this section we describe a methodology that can be used to identify radiation belt enhancement events and apply that methodology to relativistic electron fluxes measured by the LANL geosynchronous (LANL-GEO) satellite instruments. In developing this methodology, we established the following criteria for success - the methodology should:

- Identify the most intense events

- Not falsely identify data artifacts or misclassify small events
- Be quantitative and not subjective
- Establish clearly-defined onset and end times
- Not depend on any data other than the electron fluxes themselves
- Be capable of being applied to other time series of interest for space weather applications
- Be able to identify how frequent (or rare) and how severe a given event is relative to the historic record

## 2.1 The LANL-GEO Data Set

Los Alamos has operated instruments at geosynchronous orbit to measure the space environment since 1976. A new generation of instruments were deployed starting in 1989 and continue in operation today. Those instruments measure plasma (MPA [*Bame et al.*, 1993]), energetic electrons and ions (SOPA [*Belian et al.*, 1992])and relativistic electrons (ESP [*Meier et al.*, 1996]). Since 1991 there have been from 3 to 6 satellites operating simultaneously and distributed in longitude around the globe. While the measurements on each satellite are in good agreement with each other, some differences remain due to (a) the local time of the measurements - the well-known diurnal variation, (b) differences between the geographic and geomagnetic planes - which puts geographic equatorial satellites at different geomagnetic latitudes, and c) instrument responses – differences in energy passbands, efficiencies , etc. To account for these differences, we use the method described in

106 Reeves et al., [2011] to create a highly uniform, daily-averaged data set spanning

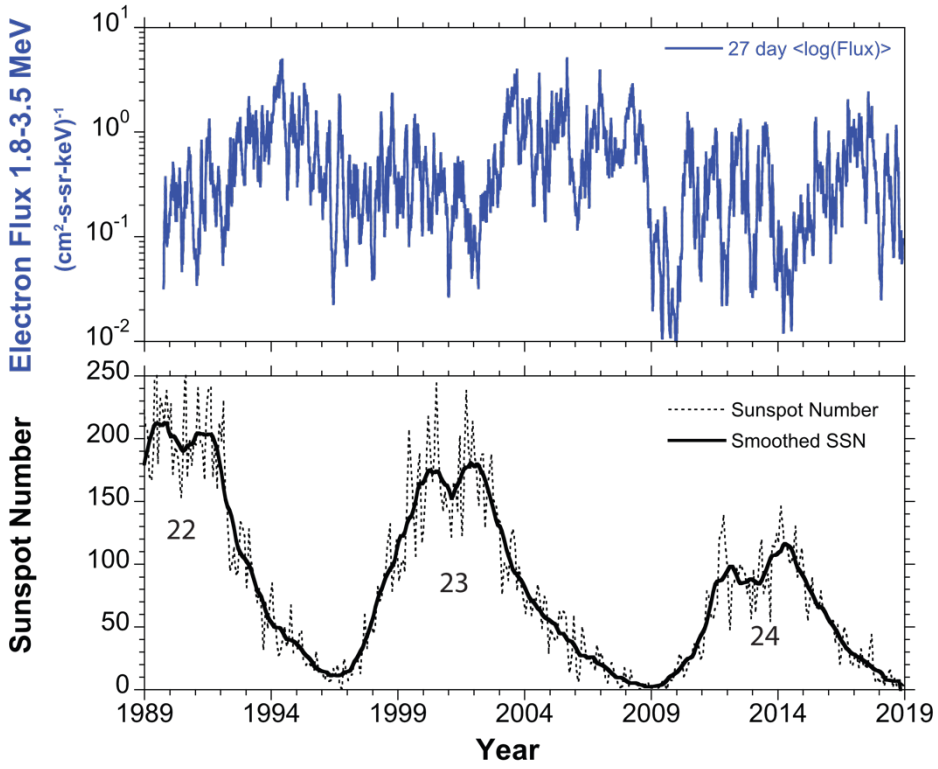


Figure 1. Running 27-day averages of MeV electron fluxes for mid 1989 through 2018 along with sunspot numbers for cycles 22 through 24.

107 nearly thirty years and three solar cycles (mid 1989 through 2018).

108 The satellites we use here are designated 1989-046, 1990-095, 1991-080, 1994-
109 084, LANL-97A, LANL-01A, LANL-02A, and LANL-04A. We first calculate daily
110 averages (median values) for each satellite. Since geosynchronous orbit covers all
111 MLT in 24-hours using a daily average essentially removes the large diurnal
112 variations. This is not, however, an absolute criterion to apply our methodology.
113 Shorter time averages are possible if diurnal variation is removed using other
114 methods [*O'Brien and McPherron*, 2003]. Next, an empirical cross-calibration is
115 applied by referencing each satellite to 1989-046 whenever both satellites acquire
116 data simultaneously. This was done for each electron energy channel measured by
117 SOPA and ESP but here we illustrate the results using a single channel designated

ESP-234 which measures electron fluxes from 1.8 to 3.5 MeV (comparable to the GOES or SAMPEX >2 MeV channels).

Figure 1 shows 27-day averages of 1.8-3.5 MeV electron fluxes and sunspot number from 1989 through 2018 in the same format as shown in Reeves et al., [*Reeves et al.*, 2011] but extended into solar cycle 24. The data set we will use for this study are the multi-satellite-daily-average 1.8-3.5 MeV electron fluxes from the LANL-GEO satellites. However, we again note that the following procedures can be applied to a variety of data sets even if the data set is not as uniform or long-duration as the one we are using.

## 2.2 Event Definition Algorithm

The algorithm we use to define a radiation belt enhancement event is quite simple.

1) The event starts when the flux exceeds a defined flux threshold
2) The event ends when the flux drops below that threshold and remains below the threshold for at least 3 days.

Here we first demonstrate the event definition using somewhat arbitrary round numbers for the threshold. NOAA uses a threshold of $10^3$ particles/(cm$^2$-s-sr) and issues an alert when flux levels exceed that threshold any time during the orbit. Therefore, daily average GOES fluxes sometimes fall below the $10^3$ particles/(cm$^2$-s-sr) flux threshold. By this definition, NOAA "events" can be separated by as little as one day. The top panel of figure 2 shows days when NOAA issued a radiation belt electron flux alert. Days with alerts are plotted in red with gray shaded backgrounds.

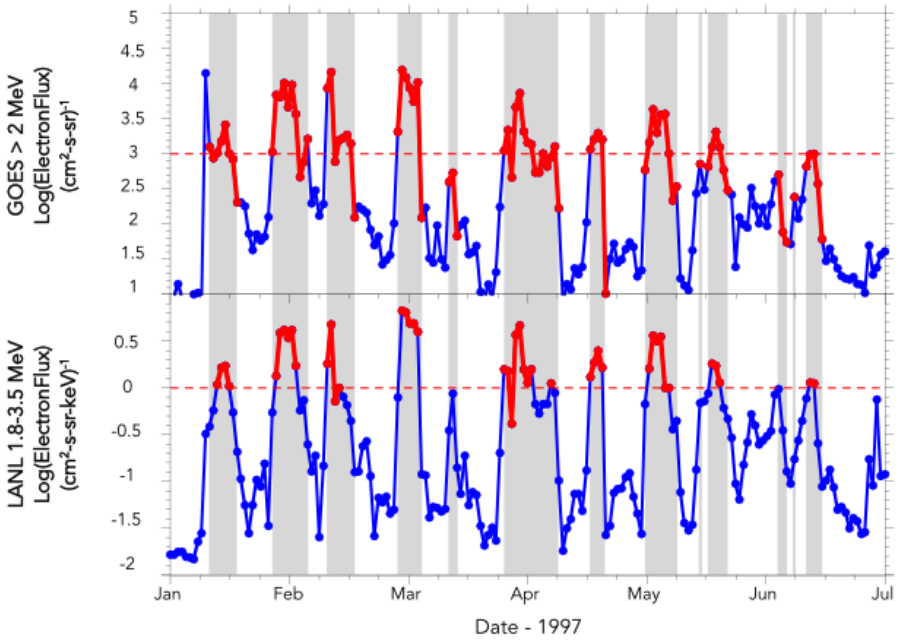


Figure 2: The top panel shows NOAA GOES >2 MeV fluxes. The NOAA threshold of $10^3$ is shown with a red dashed line and each day for which an alert was issued is also plotted in red. The bottom panel shows LANL-GEO 1.8-3.5 MeV fluxes, a the events picked by our algorithm using a flux threshold of $10^0$. The gray-shaded regions show NOAA alert days in both panels.

The bottom panel of figure 2 shows events in the LANL-GEO data that are identified by our algorithm using an arbitrary threshold of $10^0$ particles/(cm$^2$-s-sr-keV). The shaded backgrounds still indicate the NOAA alert days. Despite the somewhat arbitrary choice of flux thresholds and the difference in flux units, all of the events identified in the LANL-GEO data were also NOAA alert days.

Figure 2 also lets us address some potential ambiguities in defining the end of an event. As noted above, an event starts on the day when Flux, $F > F_{theshold}$. The event ends when $F < F_{theshold}$, meaning that previous day, when $F > F_{theshold}$, is the last day of the event. For example, the first event in the lower plot of figure 2 starts on January 13 and ends January 16 because the fluxes on January 17 were below the threshold. The events near the middle of the plot illustrate 'the 3-day rule'. The event starts on March 27 and ends on April 3. March 29 is considered part of the event because the fluxes only dropped below threshold for one day. In contrast, April 8 is considered a separate event because the fluxes for the previous four days were below threshold. This last situation is rare but should be considered, particularly for detailed case studies.

As noted, the $10^0$ particles/($cm^2$-s-sr-keV) flux threshold in figure 2 is somewhat arbitrary. If we had used a higher (lower) flux threshold in our algorithm we would have identified fewer (more) events. A more quantitative and rigorous approach is to use statistical probability distribution as described in the next section.

## 2.3 Event Definition based on Probability Distributions

In this section we examine the number of relativistic electron enhancement events (and the total number of "Days-Above-Threshold") as a function of the flux threshold used to define an event. For consistency we now apply our algorithm in the same way to both the GOES and LANL-GEO data sets. For GOES we use the daily maximum, 5-min average, >2 MeV flux from GOES East (GOES Max) which is approximately the same criteria used by NOAA to issue. For LANL-GEO we use the satellite-averaged, daily median, 1.8-3.5 MeV flux as described in section 2.1.

The probability distributions show the number of events (and Days-Above-Threshold) in any 11-year "cycle", i.e. roughly the length of a sunspot cycle. However, a "cycle" is not tied to fixed start and stop dates. Rather we use a running interval of 11-year (4,015-day) duration. There are 10,692 days in our data set. Therefore, there are approximately 6,600 "Cycles" which allows us to statistically determine mean, median, and quartiles.

The number of Days-Above-Threshold per Cycle is simply the number of days when the fluxes were greater than a specified threshold flux value (figure 3). As expected, the number of Days-Above-Threshold decreases monotonically as the threshold increases. The flattening of the distributions at low flux thresholds occurs because fluxes approach the background noise levels.

The number of Events per Cycle is defined using the algorithm described in section 2.2 and are plotted in figure 4. In contrast to Days-Above-Threshold, the number of events as a function of flux threshold have a peak. This is because, at lower flux thresholds, it is more likely that fluxes stay above the threshold for longer and

events start to merge together. At thresholds near the background level the entire data set is above threshold and constitutes a single "event". The location of the probability peak essentially defines a minimum flux threshold that can meaningfully be used to identify distinct, individual relativistic electron events.

Figures 3 and 4 show that, the two data sets have probability distributions with quite similar shapes suggesting that a probabilistic definition of events does not depend sensitively on the precise characteristics of the data sets used. With these distributions we can quantify the flux thresholds that give the same number of events or Days-Above-Threshold. For example, for GOES, the threshold that gives 100 events/cycle are 8,500 particles/(cm2-s-sr). The threshold that gives 100 events/cycle for LANL-GEO is 5.37 particles/(cm2-s-sr-keV). In this way we can directly and quantitatively compare events using the two data sets despite the differences. For example, GOES data are maximum daily fluxes and integral energy (>2 MeV) while LANL-GEO data are median daily flux and differential (1.8-3.5 MeV) but the probability distributions are insensitive to the differences in the underlying data. Even data in units of dose, dose rate, or counts/second can be directly compared using this method. Similarly, with appropriate scaling, data sets with different time resolutions can also be compared.

Of course, it is possible to define different occurrence thresholds for less common events. Based on the LANL 1.8-3.5 MeV flux distributions in figure 4 we can determine that the 10 events/cycle threshold is 17.8 particles/(cm2-s-sr-keV). The 1 event/cycle threshold is approximately 46.7 particles/(cm2-s-sr-keV). Although, with just 29.3 years in our data set, the statistics for the 1 event/cycle threshold have much larger uncertainties. Only 3 days (2 separate events) exceeded the 46.7 particles/(cm2-s-sr-keV) threshold. The maximum observed flux was 51 particles/(cm2-s-sr-keV) which occurred on July, 30 2004.

It is also possible to define different window lengths. However, a very useful feature of our methodology is that it does not depend on the 11-year window that defines a "Cycle". We are careful to include events that start before the end of the window and to not include events that start before the beginning of the window. Regardless of

214 the window length, no event is counted twice. Therefore, as long as a sliding window
215 is used, the number and timing of the identified events do not depend on the length

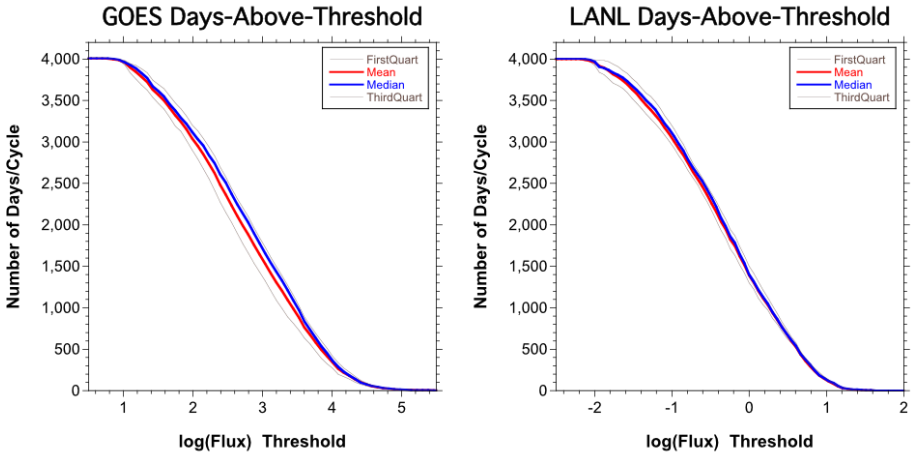


Figure 3: The number of Days-Above-Threshold per cycle based on a) GOES and b) LANL-GEO data. The GOES and LANL flux thresholds that define 1,000 Days-Above-Threshold/cycle are 3,200 particles/(cm$^2$-s-sr) and 1.9 particles/(cm$^2$-s-sr-

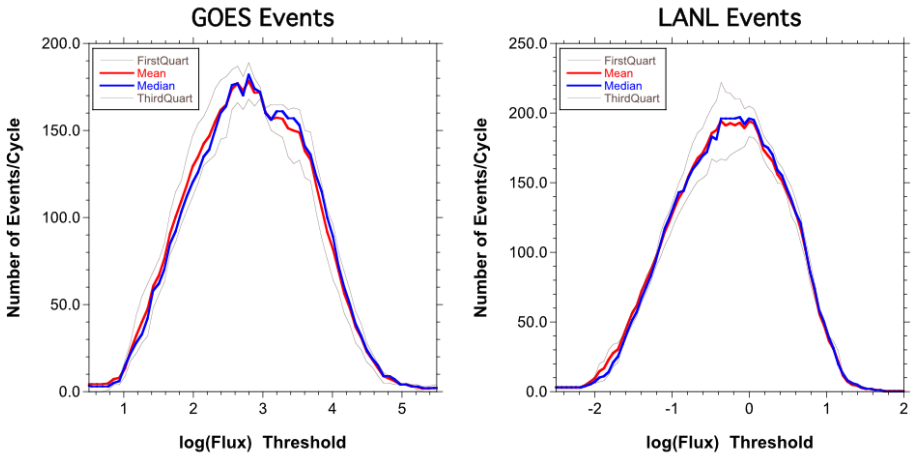


Figure 4: The number of events per cycle based on a) GOES and b) LANL-GEO data. The GOES and LANL flux thresholds that define 100 events/cycle are 8,500 particles/(cm$^2$-s-sr) and 5.37 particles/(cm$^2$-s-sr-keV) respectively.

216 of the window or its start and stop time.

## 3. Survey of Relativistic Electron Events

While the flux thresholds discussed above identify N events/cycle on average, this does not imply that events are distributed uniformly in time. The frequency and distribution of events depends on phase of the sunspot cycle and also varies from one sunspot cycle to another. The largest events tend to occur after sunspot maximum in the declining phase [e.g. *McComas et al.*, 2006; *Reeves et al.*, 2013] when long-lived equatorial coronal holes produce recurring high-speed solar wind streams (HSS) and co-rotating interaction regions (CIRs) [e.g. *Cliver*, 1995; *Hilmer et al.*, 2000; *Miyoshi and Kataoka*, 2005; *Morley et al.*, 2010; *Mouikis et al.*, 2019]. Our statistically-defined event selections confirm those results. To investigate this further, we consider the number of events each year (1990-2018) in relationship to solar cycle as defined by sunspot number.

Figure 5 shows events identified in 1994 and 2004 which were the years with the highest average fluxes and highest average solar wind speeds of solar cycles 22 and 23. Both occurred in the declining phase of the sunspot cycle (figure 1). In each plot we have indicated:

- Moderate events in green: 100/cycle, Flux > 5.37 $(cm2\text{-}s\text{-}sr\text{-}keV)^{-1}$
- Strong events in blue: 10/cycle, and, Flux > 17.8 $(cm2\text{-}s\text{-}sr\text{-}keV)^{-1}$
- Intense events in red: 1/cycle, Flux $\gtrsim$ 17.8 $(cm2\text{-}s\text{-}sr\text{-}keV)^{-1}$

Note that we intentionally avoid the term “extreme” which is reserved for events that might only occur once in 100 years such as those defined for space weather benchmarks [Space Weather Phase 1 Benchmarks, 2018].

In 1994 there were 17 moderate events and only 1 strong event. In contrast, 2004, which occurred at a similar phase of the solar cycle, had only 12 moderate events but 2 strong events and 1 intense event. The intense event in 2004 was also the highest flux observed from 1989 through 2018. We can also see that events in 2004 did not occur as regularly or last as long as events in 1994.

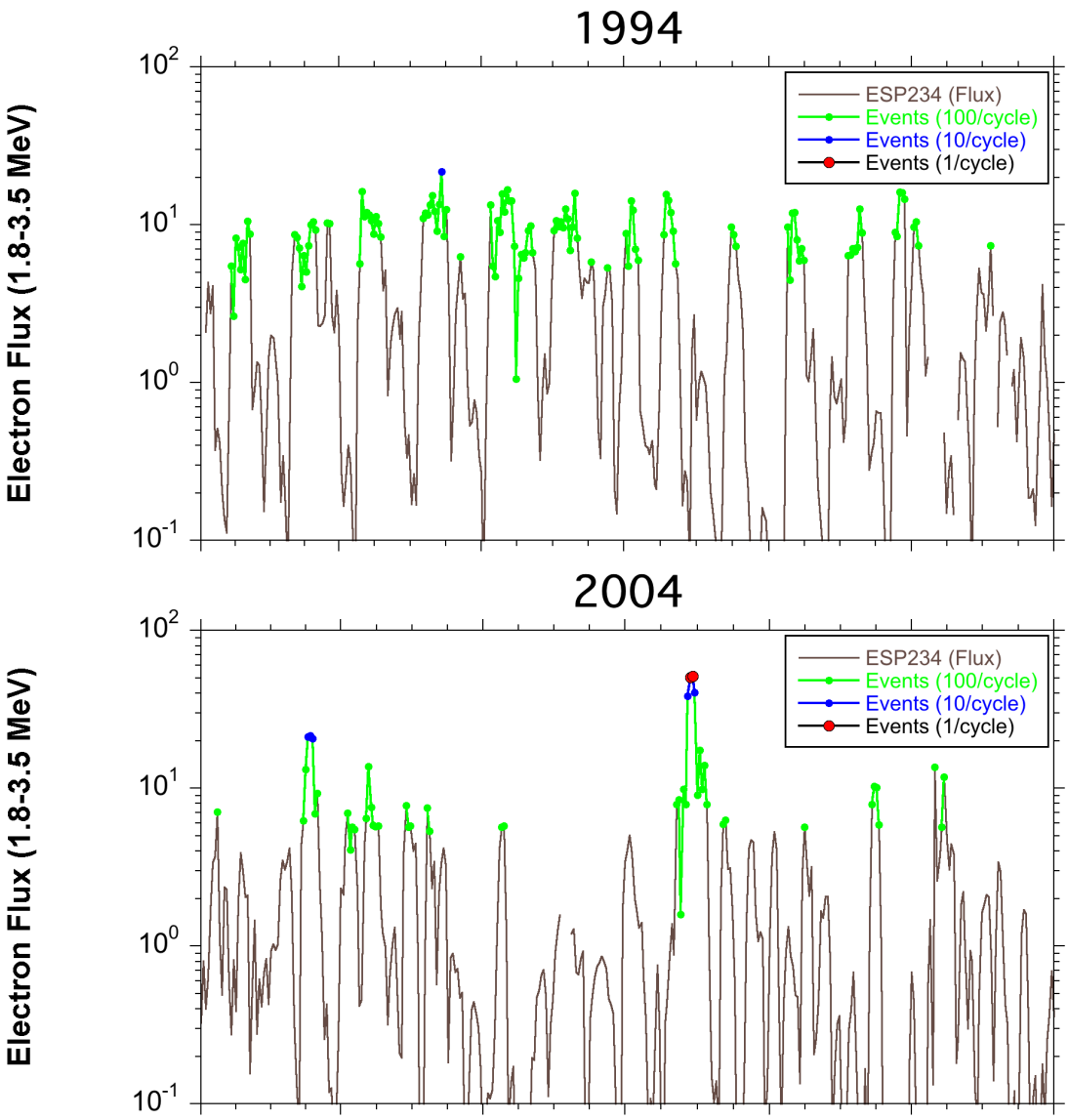


Figure 5. Relativistic electron fluxes in 1994 and 2004 during the declining phases of solar cycles 22 and 23 respectively. Moderate events (100/cycle) are identified in green, Strong events (10/cycle) are in blue, and Intense events (1/cycle) are in red.

We can further examine the distribution of events as a function of time and compare the event occurrence rates in different solar cycles. Figure 6 shows the number of moderate, strong, and intense events that occurred in each year. The bottom panels shows the mean and smoothed sunspot numbers from figure 1 for reference. The top three plots show, in blue, the number of discrete events in each category in each year (assigned to the year they start if they overlap a year boundary). They also

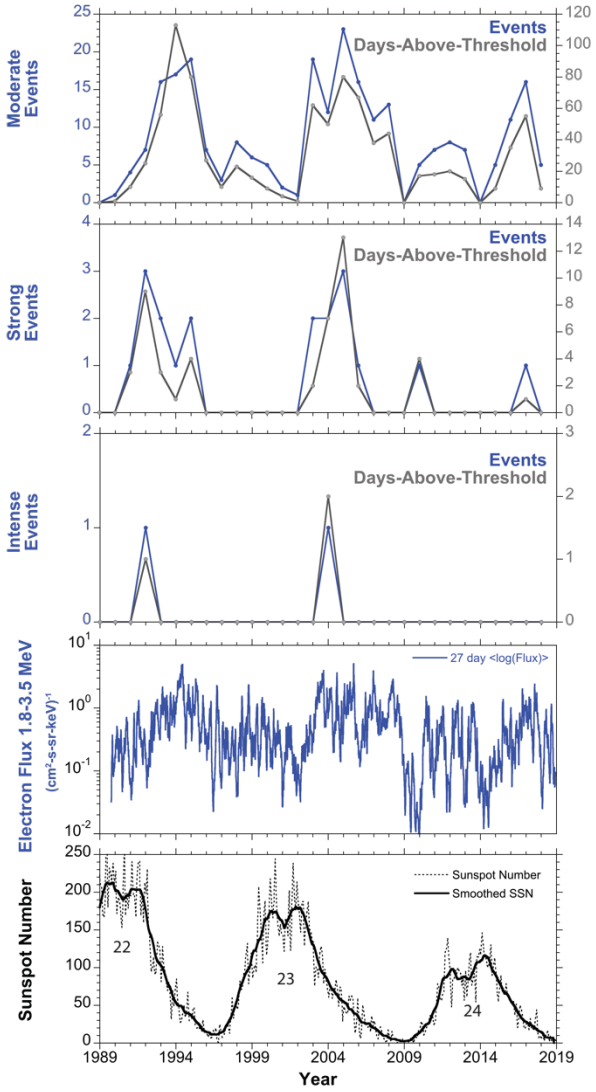


Figure 6: The occurrence rate of moderate, strong, and intense events as a function of time. The top three plots show the number of events and the number of Days-Above-Threshold in each year for each level of activity. The bottom plots reproduce figure 1 showing 1.8-3.5 MeV electron flux, and sunspot number.

250 show, in gray, the number of Days-Above-Threshold. While the two curves are well
251 correlated they do differ because even events of a given category can last a longer or
252 shorter number of days.

253 Figure 6 shows clearly that solar cycles 22 and 23 produced more, and stronger,
254 events than solar cycle 24. Solar cycles 22 and 23 were similar but also show some
255 interesting differences. Figure 6 also shows a secondary peak in moderate events
256 starting at solar minimum and continuing through the ascending phase of the solar

cycle showing how the identification of electron events described here could be used for a study of solar wind drivers without any selection bias.

The strong events show a similar time history as the moderate events but, by definition, with ten-times fewer events. Interestingly, one of the two moderate events during cycle 24 occurred in from April 8-11, 2010 during one of the deepest solar minima in the space age.

There are approximately 29.3 years in our data set. Therefore, we would expect 2.66 intense events (i.e. 1 per 11-year cycle) but there can, of course, only be an integral number of total events. In this case our algorithm identified two intense events: May 13, 1992 and July 29-30, 2004. We note, however, that a small tweak of the once-per-cycle threshold could easily have identified 3 events reflecting the uncertainty inherent when the statistics push the limits of the data.

## 4. The Van Allen Probes Era

The NASA Van Allen Probes satellites operated from Fall of 2012 to the Fall of 2019. In addition to a relatively low occurrence of sunspots, the Van Allen Probes era was characterized by relatively infrequent and less intense storms than previous solar cycles. The event identification methodology applied here allows us to more quantitatively compare the radiation belt activity during the Van Allen Probes era to previous epochs. Based on our statistics, a random 6-year period would have, on average, 54.5 moderate events, 5.5 strong events, and 0.55 intense events. We can compare that against 6 specific years of Van Allen Probes observations (January 1, 2013 through December 31, 2018). What was actually observed in those 6 years was 44 moderate events, or 80% of the average rate for all of 1989 through 2018. Looking at strong events, we find only 1 in the Van Allen Probes era which is only 18% of the average. The probability of seeing an intense event in any 6-year interval is too low to draw meaningful conclusions. A more detailed application of the methodology used here could potentially be used to help extrapolate the observations of the Van Allen Probes era to past or future epochs.

It should also be noted that, so far, we have only illustrated our event identification methodology using geosynchronous observations of ~2 MeV electrons which

represent only a small slice of the rich complexity of radiation belt dynamics. Figure 7 shows a comparison of LANL-GEO and Van Allen Probes observations for March 1 to May 15, 2017 which includes the one strong (10-per-cycle) event observed at geosynchronous orbit during the Van Allen Probes era. The figure helps put our event identification in a broader radiation belt context. The top panel shows, in black, the 2.2 MeV background-corrected electron fluxes from the MagEIS instrument on Van Allen Probes A & B [*Blake et al.*, 2013; *Spence et al.*, 2013; *Claudepierre et al.*, 2015]. Flux is plotted as a function of time only. Therefore the envelope shows the maximum flux regardless of which L-shell it is observed. The blue curve shows the LANL-GEO 1.8-3.5 MeV electron fluxes used in the preceding

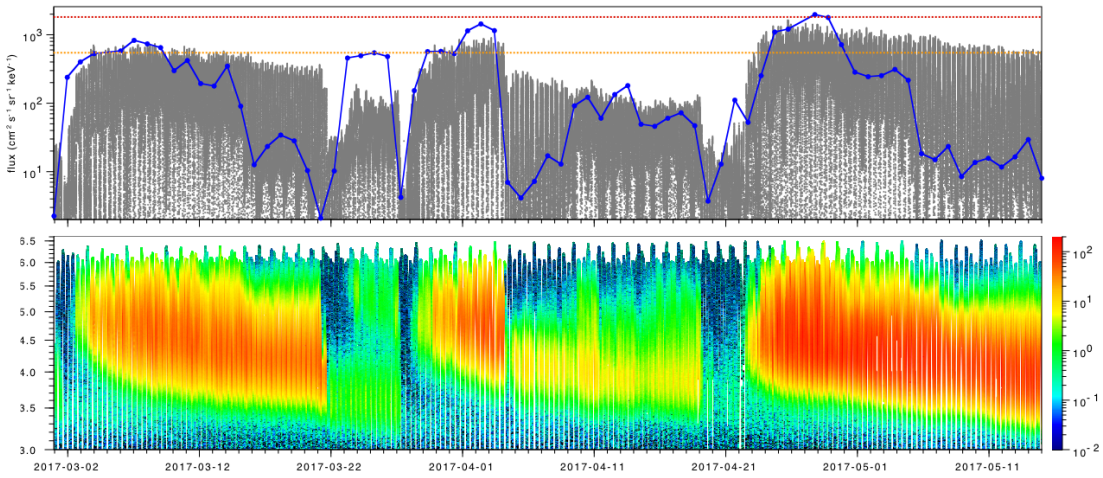


Figure 7: A comparison of LANL-GEO and Van Allen Probes observations. The top panel shows flux as a function of time for Van Allen Probes A&B MagEIS data at 2.2 MeV in black with 1.8-3.5 LANL-GEO data over plotted in blue. Thresholds for the 100 per cycle and 10 per cycle levels are shown with gray lines. The bottom panel shows the same MagEIS data plotted as a function of L-shell.

analysis. The geosynchronous moderate and strong event thresholds (5.37 and 17.8 (cm2-s-sr-keV)$^{-1}$) are shown with dashed lines. The bottom plot again shows 2.2 MeV electron data from MagEIS but now plotted as a function of both time and L-shell.

The first moderate event in this period occurred March 6 through 9. While the fluxes at geosynchronous orbit decayed more quickly than in the heart of the outer belt,

303 the geosynchronous fluxes provide a good, qualitative picture of the level of activity.
304 In the third moderate event, from March 29 through April 3, the geosynchronous
305 fluxes track the activity in the outer belt even more closely - in part because of the
306 abrupt decrease in fluxes throughout the belt at the end of the event.

307 The second moderate event, on March 25, is unusual in the sense that peak
308 geosynchronous fluxes were considerably higher than those observed by MagEIS.
309 This event is similar to that described by Baker et al. [2013] where the flux
310 enhancement was confined to higher L-shells (>4.5) and the event left the fluxes at
311 lower L-shells relatively unchanged. Nevertheless, the event on March 25 shows
312 that geosynchronous fluxes are not always a good indicator of activity throughout
313 the outer belt.

314 The final event in this interval surpassed moderate event thresholds from April 24
315 through 29 and exceeded the strong event threshold on April 27. Both the upper and
316 lower plots show that this was, indeed, a strong event both at geosynchronous orbit
317 and throughout the outer belt. Both plots also show that the flux intensification at
318 geosynchronous orbit was delayed with respect to the onset of the event. The start
319 of an 'event' - particularly a strong or intense event - will nearly always be delayed
320 relative to the onset of 'activity'.

321 Figure 7 illustrates some of the plusses and minuses of using geosynchronous data
322 to define events for the radiation belts as a whole. However, we reiterate that the
323 methodology described here is not specific to geosynchronous data but can be
324 applied to different L-shells or different energies. However, the flux thresholds that
325 define the 100, 10, and 1-per-Cycle levels will also be a function of L-shell and
326 energy. The primary advantage of the LANL-GEO data set for this purpose is the
327 duration and consistency of the data set.

## 328 5. Conclusions

329 We have presented a methodology to define strong, moderate, and intense space
330 weather events based on probability distributions. We have illustrated this

methodology using a long-duration, uniform data set of 1.8-3.5 MeV electron fluxes from multiple LANL geosynchronous satellite instruments. We established the following criteria for success: the methodology should:

- Identify the most intense events
- Not falsely identify data artifacts or misclassify small events
- Be quantitative and not subjective
- Establish clearly-defined onset and end times
- Not depend on any data other than the electron fluxes themselves
- Be capable of being applied to other time series of interest for space weather applications
- Be able to identify how frequent (or rare) and how severe a given event is relative to the historic record

In our particular use case we defined the start of an event when fluxes exceeded a particular flux threshold and the end of an event when fluxes dropped below that threshold and remained there for three or more days.

One advantage of defining events is that each event is statistically independent of all other events - as assumed in many formulations of extreme value analysis. In contrast the fluxes on any given day are well-correlated with the fluxes on preceding or following days.

We identified flux thresholds for strong, moderate, and intense events as those that produce on average 100, 10, and 1 event per 11-year time interval. (11-years is approximately one solar cycle). However, the technique is not dependent on the choice of an 11-year interval.

An advantage of using probability distributions is that they can be used to directly and quantitatively compare heterogeneous data sets. We illustrated this point by comparing 1.8-3.5 MeV LANL-GEO data (i.e. differential flux in units of (cm2-s-sr-

keV)$^{-1}$) with >2 MeV GOES data (integral flux channel in units of (cm2-s-sr)$^{-1}$). However, the technique is equally applicable to data from different orbits (e.g. GEO vs LEO), different instruments (e.g. dose or count rate data), or other space weather data sets of interest (solar wind, geomagnetic indices, etc.)

We presented a comparison of the number of relativistic electron events per year from 1990 through 2018 which span most of solar cycles 22-24. By definition there are approximately 10 times more moderate than strong events and approximately 100 times more moderate than intense events. However, in all three categories solar cycles 22 and 23 looked quite similar. In contrast solar cycle 24 showed far fewer events. Moderate events occurred at 80% of the average rate over the entire interval while strong events occurred at only 18% of the average rate. No intense events were observed.

Solar cycle 24 includes the years when the Van Allen Probes mission was operating. We also presented a comparison of geosynchronous fluxes with Van Allen Probes observations - both maximum flux/orbit and flux as a function of L-shell. As expected, geosynchronous fluxes (and events) provide a good qualitative indication of activity in the outer belt but important quantitative differences are also apparent. A more detailed comparison of Van Allen Probes data with the longer-duration geosynchronous data may allow statistical extrapolation of Van Allen Probes observations to earlier eras without such extensive measurements.

## 6. Catalog of Relativistic Electron Events

We provide here, a catalog of relativistic electron events that were identified using the methodology described in this paper:

- Moderate Events, 100-per-cycle, Flux > 5.37 (cm2-s-sr-keV)$^{-1}$
- Strong Events, 10-per-cycle, Flux > 17.8 (cm2-s-sr-keV)$^{-1}$
- Intense Events, 1-per-cycle, Flux $\gtrsim$ 46.7 (cm2-s-sr-keV)$^{-1}$

(Catalog provided in the accompanying pdf file. Catalog also available at https://zenodo.org/record/3764205 )

## Acknowledgments

This work was supported in part by RBSP–Energetic Particle, Composition, and Thermal Plasma funding under NASA's Prime contract no. NAS5-01072 and by the US Department of Energy (DOE). The GOES and LANL geosynchronous data used in this study, the probability distributions shown in figures 3 and 4, and the catalog of events used in figures 5 and 6 (also shown in section 6) are available at https://zenodo.org/record/3764205 or by request from the authors. Van Allen Probes MagEIS data is available at https://rbsp-ect.newmexicoconsortium.org/data_pub/ Sunspot numbers were obtained from WDC-SILSO, Royal Observatory of Belgium, Brussels http://www.sidc.be/silso/datafiles

# References


Anderson, B. R., et al. (2015), Acceleration and loss of relativistic electrons during small geomagnetic storms, *Geophys Res Lett*, *42*, 23, doi:10.1002/2015GL066376.

Baker, D. N., et al. (1993), An overview of the solar, anomalous, and magnetospheric particle explorer (SAMPEX) mission, *Ieee T Geosci Remote*, *31*, 3, doi:10.1109/36.225519.

Baker, D. N., et al. (2012), The relativistic electron-proton telescope (REPT) instrument on board the radiation belt storm Probes (RBSP) spacecraft: Characterization of earth's radiation belt high-energy particle populations, *Space Science Reviews*, doi:10.1007/s11214-012-9950-9.

Baker, D. N., et al. (2013), A long-lived relativistic electron storage ring embedded in Earth's outer Van Allen belt, *Science*, *340*, 6129, doi:10.1126/science.1233518.

Bame, S. J., et al. (1993), Magnetospheric plasma analyzer for spacecraft with constrained resources, *Rev. Sci. Instrum.*, *64*.

Belian, R. D., et al. (1992), High z energetic particles at geosynchronous orbit during the great solar proton event of october, 1989, *J. Geophys. Res.*, *97*, doi:10.1029/92ja01139.

Benacquista, R., et al. (2018), Variations of the electron fluxes in the terrestrial radiation belts due to the impact of corotating interaction regions and interplanetary coronal mass ejections, *Journal of Geophysical Research: Space Physics*, *123*, 2, doi:10.1002/2017ja024796.

Bingham, S. T., et al. (2019), The storm time development of source electrons and chorus wave activity during cme- and cir-driven storms, *Journal of Geophysical Research: Space Physics*, *124*, 8, doi:10.1029/2019ja026689.

Blake, J. B., et al. (1995), Ceppad: Comprehensive energetic particle and pitch angle distribution experiment on polar, *Space Sci. Rev.*, *71*.

Blake, J. B., et al. (2013), The magnetic electron ion spectrometer (MagEIS) instruments aboard the radiation belt storm Probes (RBSP) spacecraft, *Space Science Reviews*, *179*, 1-4, doi:Doi 10.1007/S11214-013-9991-8.

Borovsky, J. E., and M. H. Denton (2006), Differences between cme-driven storms and cir-driven storms, *J. Geophys. Res.*, *111*, A07S08, doi:10.1029/2005JA011447.

Claudepierre, S. G., et al. (2015), A background correction algorithm for Van Allen Probes MagEIS electron flux measurements, *Journal of Geophysical Research: Space Physics*, *120*, 7, doi:10.1002/2015JA021171.

Cliver, E. W. (1995), Solar activity and geomagnetic storms: From m regions and flares to coronal holes and cmes, *EOS Trans. AGU*, *76*.

Hilmer, R. V., et al. (2000), Enhancement of equatorial energetic electron fluxes near L=4.2 as a result of high speed solar wind streams, *J. Geophys. Res.*, *105*, doi:10.1029/1999JA000380.

Kilpua, E. K. J., et al. (2015), Unraveling the drivers of the storm time radiation belt response, *Geophys. Res. Lett.*, *42*, 9, doi:10.1002/2015gl063542.

McComas, D. J., et al. (2006), Ulysses observations of very different heliospheric structure during the declining phase of solar activity cycle 23, *Geophys. Res. Lett.*, *33*, 9, doi:10.1029/2006gl025915.

Meier, M. M., et al. (Eds.) (1996), *The energy spectrometer for particles (esp): Instrument description and orbital performance*, 203-210 pp.

Miyoshi, Y., and R. Kataoka (2005), Ring current ions and radiation belt electrons during geomagnetic storms driven by coronal mass ejections and corotating interaction regions, *Geophys. Res. Lett.*, *32*, 21, doi:10.1029/2005gl024590.

Miyoshi, Y., and R. Kataoka (2008), Flux enhancement of the outer radiation belt electrons after the arrival of stream interaction regions, *J. Geophys. Res.*, *113*, A03S09, doi:10.1029/2007JA012506.

Morley, S. K., et al. (2010), Dropouts of the outer electron radiation belt in response to solar wind stream interfaces: Global positioning system observations, *Proceedings of the Royal Society a-Mathematical Physical and Engineering Sciences*, *466*, 2123, doi:Doi 10.1098/Rspa.2010.0078.

Morley, S. K., et al. (2016), The global positioning system constellation as a space weather monitor: Comparison of electron measurements with Van Allen Probes data, *Space Weather*, *14*, 2, doi:10.1002/2015sw001339.

Mouikis, C. G., et al. (2019), The storm-time ring current response to icmes and cirs using Van Allen probe observations, *Journal of Geophysical Research: Space Physics*, *124*, 11, doi:10.1029/2019ja026695.

Moya, P. S., et al. (2017), On the effect of geomagnetic storms on relativistic electrons in the outer radiation belt: Van Allen Probes observations, *Journal of Geophysical Research: Space Physics*, *122*, 11, doi:10.1002/2017ja024735.

O'Brien, T. P., and R. L. McPherron (2003), An empirical dynamic equation for energetic electrons at geosynchronous orbit, *J. Geophys. Res.*, *108*, A3, doi:10.1029/2002ja009324.

Reeves, G., et al. (2013), Long-term variations in solar wind velocity and radiation belt electrons, *Journal of Geophysical Research: Space Physics*, *118*, 3, doi:10.1002/jgra.50126.

Reeves, G. D., et al. (1996), Los alamos geosynchronous space weather data for radiation belt modeling, in *Radiation belts: Models and standards*, edited, pp. 237-240, American Geophysical Union.

Reeves, G. D., et al. (2003), Acceleration and loss of relativistic electrons during geomagnetic storms, *Geophys. Res. Lett.*, *30*, 10, doi:10.1029/2002gl016513.

Reeves, G. D., et al. (2011), On the relationship between relativistic electron flux and solar wind velocity: Paulikas and blake revisited, *J Geophys Res-Space*, *116*, A2, doi:Doi 10.1029/2010ja015735.

Shen, X.-C., et al. (2017), Statistical study of the storm time radiation belt evolution during Van Allen Probes era: Cme- versus cir-driven storms, *Journal of Geophysical Research: Space Physics*, *122*, 8, doi:10.1002/2017ja024100.

Space Weather Operations Research and Mitigation Subcommittee - Committee on Homeland and National Security (2018), Space weather phase 1 benchmarks, Federal Register, 82 FR 7801.

Spence, H. E., et al. (2013), Science goals and overview of the radiation belt storm Probes (RBSP) energetic particle, composition, and thermal plasma (ECT) suite on nasa's Van Allen Probes mission, *Space Science Reviews*, *179*, 1-4, doi:10.1007/s11214-013-0007-5.

Turner, D. L., et al. (2019), The response of Earth's electron radiation belts to geomagnetic storms: Statistics from the Van Allen Probes era including effects from different storm drivers, *Journal of Geophysical Research: Space Physics*, *124*, 2, doi:10.1029/2018ja026066.